ORIGINAL PAPER

Analytical Model for Thermoelastic Damping in In-Plane Vibrations of Circular Cross-Sectional Micro/Nanorings with Dual-Phase-Lag Heat Conduction

Abduladheem Turki Jalil[1] · Noor Karim[2] · Ali Abdul Kadhim Ruhaima[3] · Jameel Mohammed Ameen Sulaiman[4] · Asaad Shakir Hameed[5] · Ahmed S. Abed[6] · Waleed Mohammed Khazaal[5] · Salema K. Hadrawi[7] · Yassin Rayani[8]

Abstract

Purpose The present investigation is devoted to providing two/three-dimensional (2D/3D) models for estimating the amount of thermoelastic damping (TED) in circular cross-sectional micro/nanorings by capturing the effects of size on thermal domain via dual-phase-lag (DPL) heat conduction model.

Methods To achieve the goal of the article, first of all, the equation of heat conduction derived in the framework of DPL model is solved. In this way, for 2D and 3D models of heat propagation, the temperature field in the ring is obtained in the form of infinite series. Next, by exploiting the relation of quality factor in entropy generation (EG) approach, a formulation including the two phase lag parameters of DPL model is extracted to anticipate TED value in small-sized rings with circular cross section.

Results By comparing the results of this investigation with those of studies in the literature that are based on simpler heat conduction models, a validation study is accomplished. An intensive numerical study is also performed to discern the influence of some of the most significant factors such as phase lag parameters of DPL model, vibration mode, the dimensions and ring material on TED.

Conclusion The findings reveal the noticeable effect of phase lag parameters of DPL model on the magnitude of TED in miniaturized circular cross-sectional rings, especially in smaller dimensions and higher vibration modes.

Keywords Thermoelastic damping · Dual-phase-lag model · Micro/nanorings · Circular cross section · Analytical method

✉ Abduladheem Turki Jalil
abedalazeem799@gmail.com

1   Medical Laboratories Techniques Department, Al-Mustaqbal University College, Babylon, Hilla 51001, Iraq

2   College of Medical Technology, Al-Farahidi University, Baghdad, Iraq

3   AL-Nisour University College, Baghdad, Iraq

4   Department of Dental Industry Techniques, Al-Noor University College, Bartella, Iraq

5   Mazaya University College, Nasiriyah, Iraq

6   Department of Prosthetic Dental Technology, Hilla University College, Babylon, Iraq

7   Refrigeration and Air-Conditioning Technical Engineering Department, College of Technical Engineering, The Islamic University, Najaf, Iraq

8   Department of Pharmaceutical Chemistry, College of Pharmacy, Prince Sattam Bin Abdulaziz University, Al-Kharj 11942, Saudi Arabia

Introduction

Micro/nanoelectromechanical systems (MEMS/NEMS) benefit from inimitable specifications such as diminutive size, high precision, slight energy consumption and excellent level of permanence. Consequently, the demand for using these systems in recently developed engineering tools is constantly growing. One of the most employed elements in MEMS/NEMS are circular and rectangular cross-sectional micro/nanorings. On account of their plain configuration, miniaturized rings are extensively utilized as basic constructive elements of vibrating ring gyroscopes [1, 2], rate sensors [3, 4], multi-axis angular velocity sensors [5], force sensors [6], electro-optical modulators [7], ultrasonic actuators [8], label-free sensors [9], diaphragm sensors [10], pressure and temperature sensors [11] and so on. One of the key factors in the design of these small-scaled systems is to minimize all types of energy dissipation to optimize their performance. It

has been found that thermoelastic damping (TED) is one of the definite origins of energy loss in miniaturized mechanical elements [12, 13]. Therefore, its accurate modeling in such structures is of great importance to ascertain the factors affecting energy loss, perform optimal design and maximize the quality factor.

To find the responses of mechanical systems or solve their governing equations, there are various methods such as experimental, numerical and analytical methods. Experimental methods are mostly expensive and can only be used for some situations or materials. Although numerical methods can be used for a wider range of problems, they mainly suffer from some shortcomings. They only yield approximate solutions, require some initial information at any point to start iterations, and cannot clearly show the role of influencing parameters in the solution. Analytical methods could remedy the deficiencies in experimental and numerical methods so that they can be used for a wide range of conditions and the impact of key factors on the response can be clearly seen. Therefore, the mathematical modeling of mechanical structures and the analytical solution of their governing equations have gained special importance.

For the mathematical description of heat transport in solid continua, several heat conduction theories have been proposed. The Fourier model is the first and most well-known of these models, in which the heat flux is proportional to the temperature gradient at any point of the material. On the basis of several experimental observations, the Fourier model is not able to adequately explain heat transfer in small dimensions or short times. As a result, different non-Fourier models for heat conduction have been introduced to overcome the shortcomings of the Fourier model. As one of the simplest non-Fourier models, one can mention the Lord and Shulman (LS) model which includes only one relaxation time [14]. By adding a nonlocal parameter to LS model, Guyer and Krumhansl presented a more complete model for heat conduction (GK model) [15]. By accommodating an additional phase lag parameter in the constitutive relations of LS model, Tzou established the dual-phase-lag (DPL) model to account for the small-scale effect on both size and time [16].

Based on the results reported from analytical and experimental studies, thermoelastic dissipation or thermoelastic damping is known as one of the main sources of energy loss in micro/nanostructures. This mechanism of energy dissipation can limit the quality factor of MEMS/NEMS and disrupt their optimal performance. Through the calculation of wasted energy and utilization of the entropy generation (EG) approach, Zener [17] provided the first analytical model for predicting TED value in Euler–Bernoulli beams. By separating the real and imaginary parts of the frequency, which is known as the complex frequency (CF) approach, Lifshitz and Roukes [18] established a single-term expression for estimating TED value in Euler–Bernoulli beams. It is worth mentioning that in the CF approach, both equations of motion and heat conduction must be extracted, but in the EG approach, there is no need to derive the equation of motion, which can be an advantage for this approach. In recent years, many analytical investigations have been done for mathematical modeling of the thermomechanical behavior of different structural elements such as beams [19–49], plates [50–69], shells [70–81], rings [82–90] and elastic media [91–98].

One of the first theoretical studies in the field of TED in rings has been carried out by Wong et al. [82], in which by employing the CF approach, a closed-form relation in the framework of the Fourier model has been presented for the calculation of TED value in the in-plane vibrations of silicon rings with rectangular cross section. Fang and Li [83] used the entropy EG approach and the Fourier model to attain an analytical solution for TED in rectangular cross-sectional ring resonators with 2D heat conduction. In the article published by Li et al. [84], 2D and 3D cases of the Fourier model have been utilized to appraise TED in circular cross-sectional small rings. By considering mass imperfections, Kim and Kim [85] assessed TED in toroidal solid microrings based on the three-dimensional Fourier model. According to the Fourier model, Tai and Chen [86] formulated an analytical model to evaluate TED in out-of-plane oscillations of microrings with rectangular cross section. In two similar studies conducted by Zhou et al. [87], and Zhou and Li [88], 1D and 2D cases of LS and DPL models have been applied, respectively, to emphasize the momentous impact of non-Fourier models on TED in small-sized rings with rectangular cross section. By means of 2D and 3D LS model, Kim and Kim [89] surveyed the influence of phase lag parameter on the amount of TED in circular cross-sectional micro/nanoring resonators. By means of modified couple stress theory (MCST) and nonlocal version of the DPL model, Ge and Sarkar [90] established 1D and 2D models for TED in rectangular cross-sectional miniatirized rungs.

According to the contents discussed above, thermoelastic damping (TED) plays a substantial role in the performance of structures with micro and submicron dimensions. Additionally, the literature review illuminates the inevitability of using non-Fourier heat conduction theories for precise modeling of the thermoelastic behavior of small-sized structures. Given these two points, it can be concluded that the assessment of TED in micro/nanostructures should be conducted in the purview of generalized thermoelasticity theories. The literature survey demonstrates that the analytical study on TED in micro/nanorings with circular cross-section via dual-phase-lag (DPL) model has not been conducted until now. Considering the mentioned advantages of analytical methods and EG approach, the paper at hand aims to remedy this defect

in the literature. To reach this goal, in the first step, the coupled heat conduction equation is extracted in the context of the DPL model. Asymmetric harmonic form is then considered for vibrations of the micro/nanoring resonator to determine temperature distribution for 2D and 3D models of heat conduction. On the basis of a definition of TED in the entropy generation (EG) approach, an analytical solution in the series form is established for predicting TED value in circular cross-sectional miniaturized rings by capturing the dual-phase-lagging effect. In the results section, a validation study is first performed to ensure the correctness of the presented model by comparing the results with existing works. Next, a convergence analysis is carried out to ascertain the sufficient number of terms of the obtained solution to arrive at a convergent result. The final step is to conduct a parametric study for highlighting the sensitivity of TED to some influencing factors like phase lag parameters of the DPL model, vibration mode, the dimensions and ring material.

Basic Relationships of Dual-Phase-Lag (DPL) Heat Conduction Model

On the basis of the DPL heat conduction model for isotropic materials, the heat flux vector $\boldsymbol{q}$ and gradient of temperature increment $\nabla\vartheta$ are related through the following relation [3]:

$$\boldsymbol{q} + \tau_{\mathrm{q}}\frac{\partial \boldsymbol{q}}{\partial t} = -k\nabla\vartheta - k\tau_{\mathrm{T}}\frac{\partial \nabla\vartheta}{\partial t}, \tag{1}$$

in which k denotes thermal conductivity. In addition, material constants τ_{q} and τ_{T} are called phase lag of heat flux and phase lag of temperature gradient. Moreover, symbol ∇ represents the Laplace operator. The variable $\vartheta = T - T_0$ is also the temperature variation with T and T_0 as instantaneous and environmental temperatures, respectively. Note that when τ_{T} vanishes, the heat conduction equation of the DPL model corresponds to that of the LS model. Furthermore, in the absence of phase lag parameters τ_{q} and τ_{T}, Eq. (1) reduces to the constitutive relation of the Fourier model. For an isotropic material, the equation of conservation of energy is given by [3]:

$$-\nabla.\boldsymbol{q} = \rho c_{\mathrm{v}}\frac{\partial \vartheta}{\partial t} + T_0\beta\frac{\partial e}{\partial t}, \tag{2}$$

where ρ and c_{v} refer to the mass density and specific heat per unit mass, respectively. Additionally, parameter $\beta = E\alpha/(1-2\nu)$ defines thermal modulus. Variable e is also a volumetric strain. Lastly, by omitting heat flux $\boldsymbol{q}$ from Eqs.

(1) and (2), equation of heat conduction in the framework of DPL models is obtained as follows:

$$k\left(1 + \tau_{\mathrm{T}}\frac{\partial}{\partial t}\right)\nabla^2\vartheta = \left(1 + \tau_{\mathrm{q}}\frac{\partial}{\partial t}\right)\left(\rho c_{\mathrm{v}}\frac{\partial \vartheta}{\partial t} + T_0\beta\frac{\partial e}{\partial t}\right). \tag{3}$$

Coupled Thermoelastic Equation of Circular Cross-Sectional Rings Based on DPL Model

Figure 1 displays the schematic view and coordinate system of a circular cross-sectional ring with mean radius R_0 and cross-sectional radius r_0. The global and local coordinates are defined by (R, θ, Z) and (x, y, z), respectively. Moreover, the parameter ϕ denotes the local angle. By considering these definitions, the circumferential strain can be expressed by [84]:

$$\varepsilon_{\theta\theta} = -\frac{x}{R_0^2}\left(u + \frac{\partial^2 u}{\partial\theta^2}\right), \tag{4}$$

in which u represents the radial displacement. Based on coupled thermoelastic constitutive relation, the following relation can be obtained:

$$\varepsilon_{\theta\theta} = \frac{\sigma_{\theta\theta}}{E} + \alpha\vartheta, \tag{5}$$

where $\sigma_{\theta\theta}$ indicates circumferential normal stress. Using the above relation, one can get:

$$\sigma_{\theta\theta} = E\varepsilon_{\theta\theta} - E\alpha\vartheta. \tag{6}$$

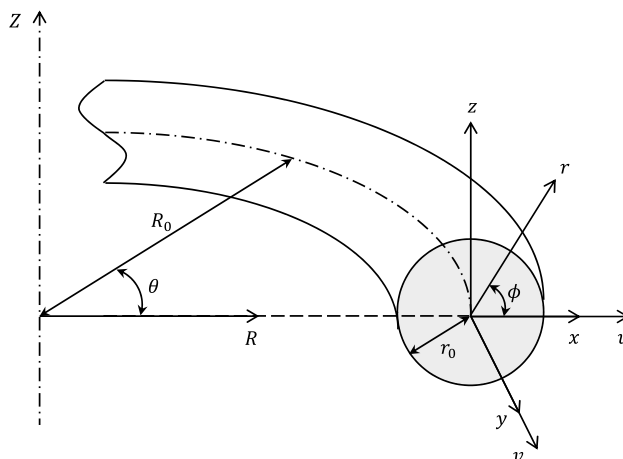Other thermoelastic constitutive relations can be expressed as follows:

Fig. 1 Schematic view and coordinate system of a circular cross-sectional ring

$$\varepsilon_{RR} = \varepsilon_{zz} = -v \frac{\sigma_{\theta\theta}}{E} + \alpha \vartheta. \tag{7}$$

Substitution of Eqs. (4) and (6) in the above equation gives:

$$e = \varepsilon_{RR} + \varepsilon_{\theta\theta} + \varepsilon_{zz} = (2v - 1) \frac{x}{R_0^2} \left(u + \frac{\partial^2 u}{\partial \theta^2} \right) + 2(1 + v)\alpha\vartheta. \tag{8}$$

By inserting Eq. (8) into Eq. (3) and simplifying the result, the equation of heat conduction becomes:

$$\chi \left(1 + \tau_T \frac{\partial}{\partial t}\right) \nabla^2 \vartheta - \left[1 + \frac{2(1+v)}{1-2v} \Delta_E\right] \left(1 + \tau_q \frac{\partial}{\partial t}\right) \frac{\partial \vartheta}{\partial t}$$
$$= -\frac{\Delta_E}{\alpha} \left(1 + \tau_q \frac{\partial}{\partial t}\right) \frac{\partial}{\partial t} \left[\frac{x}{R_0^2} \left(u + \frac{\partial^2 u}{\partial \theta^2}\right)\right], \tag{9}$$

with $\chi = k/\rho c_v$ and $\Delta_E = E\alpha^2 T_0/\rho c_v$. Due to the small amount of parameter Δ_E for most materials (i.e. $\Delta_E \ll 1$), Eq. (9) can be replaced with the following equation:

$$\chi \left(1 + \tau_T \frac{\partial}{\partial t}\right) \nabla^2 \vartheta - \left(1 + \tau_q \frac{\partial}{\partial t}\right) \frac{\partial \vartheta}{\partial t}$$
$$= -\frac{\Delta_E}{\alpha} \left(1 + \tau_q \frac{\partial}{\partial t}\right) \frac{\partial}{\partial t} \left[\frac{x}{R_0^2} \left(u + \frac{\partial^2 u}{\partial \theta^2}\right)\right]. \tag{10}$$

Temperature increment ϑ and radial displacement u can be expressed as follows [84]:

$$\vartheta(R, \theta, z, t) = \Theta_0(R, \theta, z)e^{i\omega_n t}, u(\theta, t) = U_n \sin(n\theta)e^{i\omega_n t}, \tag{11}$$

in which ω_n refers to the n-th vibration frequency, which is calculated from the following relation [84]:

$$\omega_n = \frac{n(n^2 - 1)}{\sqrt{n^2 + 1}} \sqrt{\frac{EI}{\rho A R_0^4}} (n \geq 2), \tag{12}$$

with $I = \pi r_0^4/4$ and $A = \pi r_0^2$ as the moment of inertia and cross-sectional area, respectively. From Fig. 1, one can write:

$$x = r \sin \phi, z = r \cos \phi. \tag{13}$$

By substituting Eqs. (11) and (13) into Eq. (10) and sorting the result, one can achieve the following equation:

$$\chi \left(1 + i\omega_n \tau_T\right) \nabla^2 \Theta_0 - \left(i\omega_n - \tau_q \omega_n^2\right) \Theta_0$$
$$= -\frac{\Delta_E}{\alpha} \frac{r \sin \phi}{R_0^2} \left(1 - n^2\right) U_n \sin(n\theta) \left(i\omega_n - \tau_q \omega_n^2\right). \tag{14}$$

Three-dimensional form of the Laplace operator can be written as follows:

$$\nabla^2_{3D}\Theta_0 = \frac{\partial^2 \Theta_0}{\partial R^2} + \frac{1}{R} \frac{\partial \Theta_0}{\partial R} + \frac{1}{R^2} \frac{\partial^2 \Theta_0}{\partial \theta^2} + \frac{\partial^2 \Theta_0}{\partial z^2}. \tag{15}$$

By referring to Eq. (13) and relation $R = R_0 + x$, and considering the fact that in thin rings $R_0 \gg x$, Eq. (15) takes the following form:

$$\nabla^2_{3D}\Theta_0 = \frac{\partial^2 \Theta_0}{\partial r^2} + \frac{1}{r} \frac{\partial \Theta_0}{\partial r} + \frac{1}{R_0^2} \frac{\partial^2 \Theta_0}{\partial \theta^2} + \frac{1}{r^2} \frac{\partial^2 \Theta_0}{\partial \phi^2}. \tag{16}$$

In the case of 2D heat conduction, the temperature gradient along the circumferential direction is neglected. Hence, the Laplace operator can be written as:

$$\nabla^2_{2D}\Theta_0 = \frac{\partial^2 \Theta_0}{\partial r^2} + \frac{1}{r} \frac{\partial \Theta_0}{\partial r} + \frac{1}{r^2} \frac{\partial^2 \Theta_0}{\partial \phi^2}. \tag{17}$$

According to the relationship between global and local coordinates, $\Theta_0(r, \theta, \phi)$ can be used instead of $\Theta_0(R, \theta, z)$. By assuming adiabatic conditions on the outer surface of the ring and continuity of temperature in all angles θ and ϕ, the thermal boundary conditions can be expressed as follows:

$$\frac{\partial \Theta_0}{\partial r}\left(r = r_0\right) = 0, \Theta_0(r, \theta, \phi) = \Theta_0(r, \theta + 2\pi, \phi),$$
$$\Theta_0(r, \theta, \phi) = \Theta_0(r, \theta, \phi + 2\pi). \tag{18}$$

By considering the above relations and inserting Eq. (16) into Eq. (14), the temperature distribution is derived as follows [84]:

$$\Theta_0(r, \theta, \phi) = \sum_{m=0}^{\infty} \sum_{j=1}^{\infty} C_{jm} J_1 \left(\frac{a_j}{r_0} r\right) \sin(m\theta) \sin\phi, \tag{19}$$

in which J_1 refers to the first-order Bessel function of the first kind. To attain the amount of coefficients a_j, the first relation of Eq. (18) is employed. By substituting Eq. (19) into the mentioned relation and exploiting the properties of Bessel functions, one can get:

$$J_0(a_j) = J_2(a_j). \tag{20}$$

Thus, a_j is equal to the j-th root of the above equation. The first ten roots of this equation are listed in Table 1. To extract the coefficients C_{jm}, the orthogonality property of Bessel and trigonometric functions is used. By inserting Eq. (19) into (14), multiplying the result by $r J_1 \left(\frac{a_k}{r_0} r\right) \sin(n\theta) \sin\phi$, and integrating the outcome in the range of $(0, r_0)$, $(0, 2\pi)$ and $(0, 2\pi)$, it is finally obtained that:

$$C_{kn} = \frac{\Delta_E}{\alpha} \frac{2r_0}{R_0^2}(1 - n^2)$$
$$U_n \frac{1}{(a_k^2 - 1)J_1(a_k)} \frac{(i\omega_n - \tau_q \omega_n^2)\tau_k}{(1 + i\omega_n \tau_T)(1 + \delta_{kn}^2) + (i\omega_n - \tau_q \omega_n^2)\tau_k}, \tag{21}$$

Table 1 The first ten terms of a_k and G_k for the rings with circular cross-section

k	a_k	G_k
1	1.841	0.987
2	5.331	0.010
3	8.536	1.528×10^{-3}
4	11.706	4.292×10^{-4}
5	14.864	1.647×10^{-4}
6	18.016	7.618×10^{-5}
7	21.164	3.996×10^{-5}
8	24.311	2.294×10^{-5}
9	27.457	1.409×10^{-5}
10	30.602	9.132×10^{-6}

where

$$\delta_{kn} = \frac{n r_0}{a_k R_0} \tag{22a}$$

$$\tau_k = \frac{r_0^2}{\chi a_k^2}. \tag{22b}$$

Hence, the final form of temperature distribution can be expressed via the following relation:

$$\Theta_0(r,\theta,\phi) = \frac{\Delta_E}{\alpha} \frac{2 r_0}{R_0^2} \left(1 - n^2\right) U_n \sin(n\theta) \sin\phi \sum_{k=1}^{\infty} \frac{J_1\left(\frac{a_k}{r_0} r\right)}{(a_k^2 - 1) J_1(a_k)} \frac{\left(i\omega_n - \tau_q \omega_n^2\right) \tau_k}{\left(1 + i\omega_n \tau_T\right)\left(1 + \delta_{kn}^2\right) + \left(i\omega_n - \tau_q \omega_n^2\right) \tau_k}. \tag{23}$$

By separating the real and imaginary parts of the above relation, one can obtain:

$$Re(\Theta_0) = \frac{\Delta_E}{\alpha} \frac{2 r_0}{R_0^2} \left(1 - n^2\right) U_n \sin(n\theta) \sin\phi$$

$$\mathrm{Re}(\Theta_0) = \frac{\Delta_E}{\alpha} \frac{2 r_0}{R_0^2} \left(1 - n^2\right) U_n \sin(n\theta) \sin\phi$$

$$\sum_{k=1}^{\infty} \frac{J_1\left(\frac{a_k}{r_0} r\right)}{(a_k^2 - 1) J_1(a_k)} \frac{-\tau_k \tau_q \omega_n^2 \left(1 + \delta_{kn}^2 - \tau_k \tau_q \omega_n^2\right) + \tau_k \omega_n^2\left[\left(1 + \delta_{kn}^2\right)\tau_T + \tau_k\right]}{\left(1 + \delta_{kn}^2 - \tau_k \tau_q \omega_n^2\right)^2 + \left[\left(1 + \delta_{kn}^2\right)\tau_T + \tau_k\right]^2 \omega_n^2} \tag{24a}$$

$$\mathrm{Im}(\Theta_0) = \frac{\Delta_E}{\alpha} \frac{2 r_0}{R_0^2} \left(1 - n^2\right) U_n \sin(n\theta) \sin\phi$$

$$\sum_{k=1}^{\infty} \frac{J_1\left(\frac{a_k}{r_0} r\right)}{(a_k^2 - 1) J_1(a_k)} \frac{\tau_k \omega_n \left(1 + \delta_{kn}^2 - \tau_k \tau_q \omega_n^2\right) + \tau_k \tau_q \omega_n^3\left[\left(1 + \delta_{kn}^2\right)\tau_T + \tau_k\right]}{\left(1 + \delta_{kn}^2 - \tau_k \tau_q \omega_n^2\right)^2 + \left[\left(1 + \delta_{kn}^2\right)\tau_T + \tau_k\right]^2 \omega_n^2} \tag{24b}$$

Derivation of a Relationship to Compute the Value of TED

According to the entropy generation (EG) approach, TED value is determined by:

$$\text{TED} = \frac{1}{2\pi} \frac{\Delta W}{W}, \tag{25}$$

where ΔW is the wasted energy through entropy generation per cycle of vibration and W stands for the maximum strain energy stored in the ring at the time of vibration. The wasted energy in a vibrating structure with volume Ω during a cycle is given by [99]:

$$\Delta W = -\pi \iiint_{\Omega} \tilde{\sigma}_{ij} \mathrm{Im}\left(\tilde{\varepsilon}_{ij}^{\text{thermal}}\right) d\Omega, \tag{26}$$

where the symbol $\sim$ refers to the maximum value of a variable per cycle of oscillation. The value of W is also given by:

$$W = \frac{1}{2} \iiint_{\Omega} \tilde{\sigma}_{ij} \tilde{\varepsilon}_{ij} d\Omega. \tag{27}$$

In a ring, the amount of ΔW is estimated by the following relation:

$$\Delta W = -\pi \iiint_{\Omega} \tilde{\sigma}_{\theta\theta} \mathrm{Im}\left(\alpha \Theta_0\right) d\Omega. \tag{28}$$

In addition, the maximum stored energy W can be determined by:

$$W = \frac{1}{2} \iiint_\Omega \tilde{\sigma}_{\theta\theta} \tilde{\varepsilon}_{\theta\theta} d\Omega. \tag{29}$$

By utilizing Eqs. (4), (6) and (11) and disregarding thermal stress, one can arrive at the following relation:

$$\tilde{\sigma}_{\theta\theta} = -\frac{Ex}{R_0^2}\left(1 - n^2\right)U_n \sin(n\theta) = -\frac{Er\sin\phi}{R_0^2}\left(1 - n^2\right)U_n \sin(n\theta). \tag{30}$$

Similarly, one can obtain:

$$\tilde{\varepsilon}_{\theta\theta} = -\frac{x}{R_0^2}\left(1 - n^2\right)U_n \sin(n\theta) = -\frac{r\sin\phi}{R_0^2}\left(1 - n^2\right)U_n \sin(n\theta). \tag{31}$$

For a toroidal ring, one can write:

$$d\Omega = (R + x)d\theta.rd\phi.dr = (R + r\sin\phi)d\theta.rd\phi.dr. \tag{32}$$

By inserting Eqs. (30)–(32) into Eq. (29) and integrating the result over $0 \le \theta \le 2\pi$, $0 \le \phi \le 2\pi$ and $0 \le r \le r_0$, the maximum stored energy W is obtained as:

$$W = \frac{\pi E I R_0}{2}\left[\frac{\left(1 - n^2\right)U_n}{R_0^2}\right]^2. \tag{33}$$

Through a similar method, substitution of Eqs. (24b), (30) and (32) into Eq. (28) and integration over the entire ring volume gives:

$$\Delta W = 2\pi\Delta_{\mathrm{E}}.W.\sum_{k=1}^{\infty} G_k \frac{\tau_k\omega_n\left(1 + \delta_{kn}^2 - \tau_k\tau_q\omega_n^2\right) + \tau_k\tau_q\omega_n^3\left[\left(1 + \delta_{kn}^2\right)\tau_{\mathrm{T}} + \tau_k\right]}{\left(1 + \delta_{kn}^2 - \tau_k\tau_q\omega_n^2\right)^2 + \left[\left(1 + \delta_{kn}^2\right)\tau_T + \tau_k\right]^2\omega_n^2}, \tag{34}$$

in which G_k is a weight coefficient that is defined by:

$$G_k = \frac{8}{a_k^2\left(a_k^2 - 1\right)}. \tag{35}$$

The values G_k for the first ten terms are presented in Table 1.

Finally, by inserting Eq. (34) into Eq. (25), the relation for computing TED value in circular cross-sectional micro/nanorings, which includes the phase lag parameters of the DPL model is obtained as follows:

$$TED = \Delta_E \sum_{k=1}^{\infty} G_k \frac{\tau_k\omega_n\left(1 + \delta_{kn}^2 - \tau_k\tau_q\omega_n^2\right) + \tau_k\tau_q\omega_n^3\left[\left(1 + \delta_{kn}^2\right)\tau_T + \tau_k\right]}{\left(1 + \delta_{kn}^2 - \tau_k\tau_q\omega_n^2\right)^2 + \left[\left(1 + \delta_{kn}^2\right)\tau_T + \tau_k\right]^2\omega_n^2} \tag{36}$$

It is worth noting that in the absence of phase lags τ_q and τ_T, above equation is reduced to the relation derived by Li et al. [84] by means of the Fourier model. Also, by

dropping the terms including τ_T, the relationship developed in this work corresponds to that established by Kim and Kim [89] according to single-phase-lag (SPL) or LS model. These comparisons can be evidence to verify the presented formulation.

Numerical Results and Discussion

In this section, firstly, a comparison study is carried out to examine the validity and accuracy of the developed formulation in this research. For this purpose, the results of the present study for a specific case are compared with those reported by Kim and Kim [89]. It should be noted that for estimating the amount of TED in 2D model, it is enough that the terms caused by the derivatives in the circumferential direction are removed. In other words, the value of δ_{kn} is set equal to zero in the calculations. In the article of Kim and Kim [89], TED in rings with circular cross section has been assessed on the basis of LS model. Accordingly, the outcomes of the current article can be compared with those of [89] by setting $\tau_T = 0$ in the formulation presented in Eq. (36). In addition, to compare the results of this paper with the investigation of Li et al. [84], which has been done in the framework of the Fourier model, the terms including τ_q and τ_T in Eq. (36) should be neglected. In Fig. 2, the variation of TED in a ring made of silicon (Si) with respect to the vibration mode n is depicted. Material constants of Si are presented in Table 2. The geometric
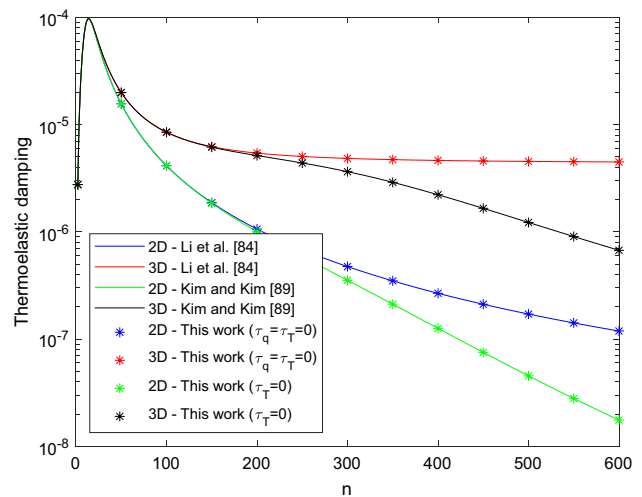

Fig. 2 Comparison study for a ring made of silicon with geometric properties $r_0 = 1\,\mu m$ and $R_0 = 50\,\mu m$

Table 2 Material constants of silicon (Si) at a reference temperature $T_0 = 293K$ [89]

E(GPa)	$\rho\left(\text{kg m}^{-3}\right)$	$k\left(\text{W m}^{-1}\text{ K}^{-1}\right)$	$\alpha\left(10^{-6}\text{ K}^{-1}\right)$	$c_v\left(\text{J kg}^{-1}\text{ K}^{-1}\right)$	τ_q(ps)
165.9	2330	156	2.59	713	3.95649

parameters of the ring are also considered as $r_0 = 1\,\mu\text{m}$ and $R_0 = 50\,\mu\text{m}$. As can be seen, the outcomes of the present work are consistent with those of [89], which can be a sign of the integrity and veracity of the model derived in this article.

In the following, several numerical examples are provided to appraise the sensitivity of TED value to some key factors such as phase lag parameters of DPL model, number of vibration mode, 2D and 3D cases of heat transfer, geometrical characteristics and material. Mechanical and thermal properties of gold (Au), copper (Cu), lead (Pb) and silver (Ag) at $T_0 = 300K$ are presented in Table 3 [3]. Except for the cases where the effect of the material on TED is investigated, the rest of the results are given for the rings made of gold.

In Fig. 3, the effect of the number of terms considered in Eq. (36) on the value of TED as a function of vibration mode number is analyzed. In this figure, the curves are plotted for 2D and 3D models and for solutions including only one term and the first ten terms. Also, the geometrical properties of the ring are assumed to be $r_0 = 200\text{nm}$ and $R_0 = 20r_0$. As it is clear, the difference of the results obtained from considering the first ten terms and only one term is insignificant and the graphs of these two cases are almost identical.

For 2D and 3D models of heat conduction, Fig. 4 indicates the ratio of TED calculated by the first ten terms to that estimated by the single term. As can be seen, the difference between the results of these two cases is less than one percent. This difference is much smaller for lower vibration modes. Based on Figs. 3 and 4, it can be concluded that considering the first ten terms is enough to achieve convergent results. Therefore, in the following figures, the results are drawn for the first ten terms of the provided solution.

Figures 5a, b illustrate the impact of the Fourier and DPL models on the variations of TED with mode number for cases $R_0 = 20r_0$ and $R_0 = 100r_0$, respectively. To achieve

these figures, it is assumed that $r_0 = 50\text{nm}$. Based on these graphs, it can be concluded that, in general, DPL model predicts lower values for TED than the Fourier model. When the dimensions of the ring are larger (i.e. $R_0 = 100r_0$), this result can be stated with more certainty and for almost all vibration modes. The physical interpretation of this result is that DPL model anticipates a wave-like characteristic for heat propagation with finite velocity, whereas the Fourier model estimates that thermal signals transfer in solids through diffusion phenomenon. Owing to finite speed of heat
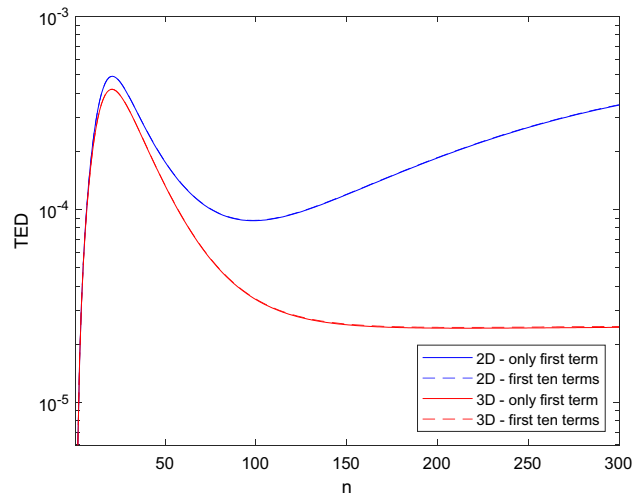

Fig. 3 Variations of TED in terms of vibration mode number for only one term and the first ten terms of presented solution for $r_0 = 200$ nm and $R_0 = 20r_0$

Table 3 Properties of gold (Au), copper (Cu), lead (Pb) and silver (Ag) at a reference temperature $T_0 = 300K$ [3]

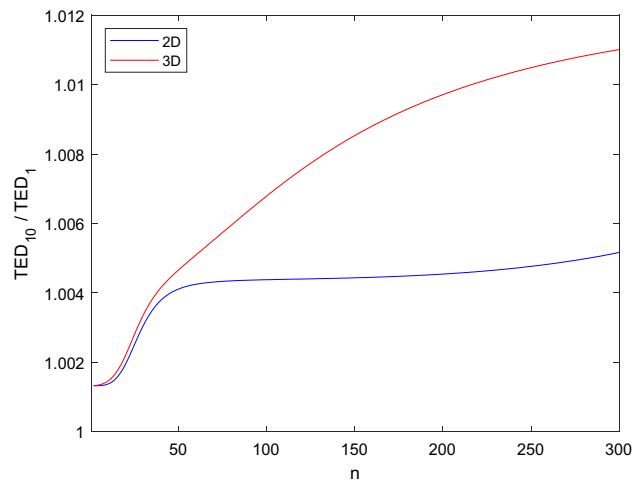| Material constant	Au	Cu	Pb	Ag
E(GPa)	79	110	16	76
$\rho\left(\text{kg m}^{-3}\right)$	19,300	8940	11,340	10,500
$k\left(\text{W m}^{-1}\text{ K}^{-1}\right)$	315	386	35.3	430
$\alpha\left(10^{-6}\text{ K}^{-1}\right)$	14.2	16.5	28.9	19.5
$c_v\left(\text{J kg}^{-1}\text{K}^{-1}\right)$	129.1	385.9	128	285.7
τ_q(ps)	0.7438	0.4348	0.1670	0.7438
τ_T(ps)	89.286	70.833	12.097	89.286

Fig. 4 The ratio of TED with the first ten terms to TED with only the first term for $r_0 = 200\text{nm}$ and $R_0 = 20r_0$
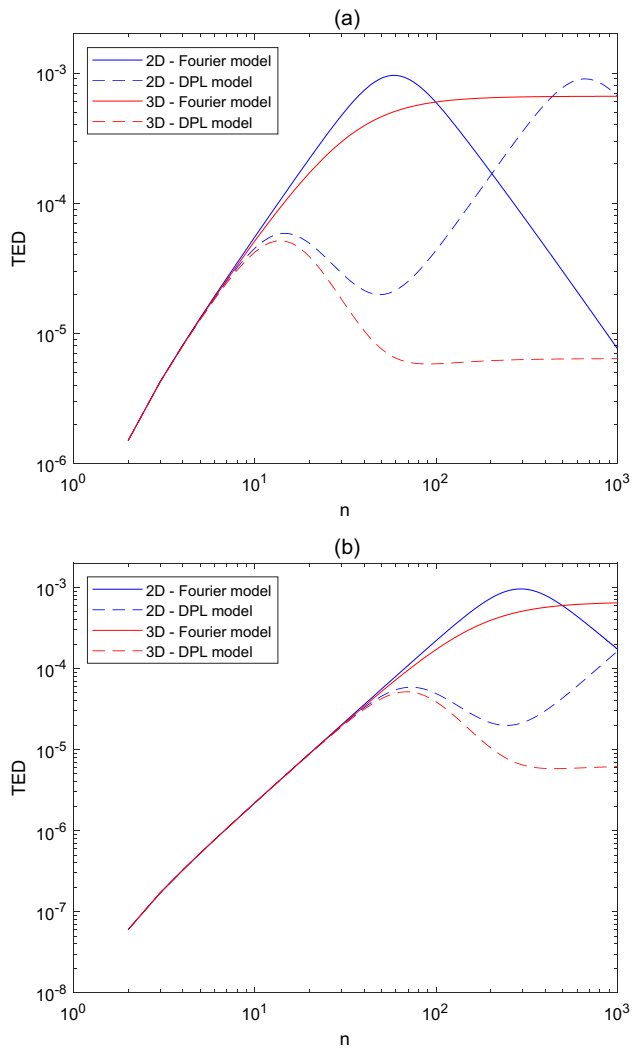
Fig. 5 The influence of the Fourier and DPL models on the variations of TED versus vibration mode number for $r_0 = 50$nm **a** $R_0 = 20r_0$ **b** $R_0 = 100r_0$

Fig. 6 The influence of the Fourier and DPL models on the variations of TED versus vibration mode number for $r_0 = 1$ μm **a** $R_0 = 20r_0$ **b** $R_0 = 100r_0$

transfer in DPL model, heat induced by a nonuniform stress field has no adequate time to propagate during the vibration of structure, which alleviates energy loss originated by thermoelastic damping. Accordingly, TED values predicted by the DPL model are lower than those of the Fourier model. Another conclusion that can be drawn from these curves is that for a wide range of vibration modes, TED value calculated by 3D model is smaller than that determined by the 2D model. It is also observed that when the size of the ring becomes larger (i.e. $R_0 = 100r_0$), the difference between the Fourier and DPL models as well as the difference between 2 and 3D cases of heat conduction lessen for a wider range of vibration mode number.

Figures 6a, b are drawn under the same conditions as Fig. 5a, b. The only difference is that in these figures $r_0 = 1$ μm is considered. In other words, these diagrams are plotted
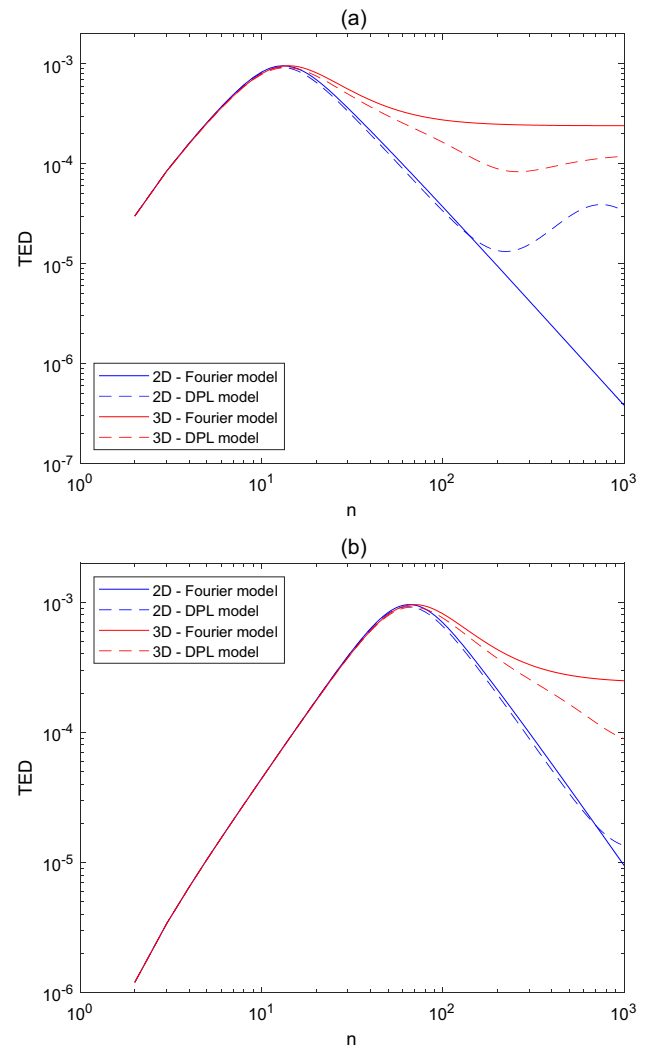
for the rings with larger dimensions than the previous figure. Comparing these diagrams with the curves in the previous figure shows that the effect of the DPL model on TED is almost the same for both cases $r_0 = 50$nm and $r_0 = 1$ μm, that is, for a large range of vibration modes, TED value calculated by the DPL model is lower than that obtained by means of the Fourier model. These graphs also illustrate that 2D and 3D models have different effects on cases $r_0 = 50$nm and $r_0 = 1$ μm, so that unlike the case $r_0 = 50$nm, 3D model predicts more values for TED in case $r_0 = 1\mu m$. According to what was said before, to arrive at the results of 2D model, term δ_{kn} in Eq. (36) should be set equal to zero. Thus, one can state that the difference between 2 and 3D models gets negligibly small as the variable δ_{kn} takes an insignificant value. In view of the relation $\delta_{kn} = (n/a_k)(r_0/R_0)$, this issue happens when either the number of vibration mode n is low

or the amount of ratio r_0/R_0 is very small. This can be readily seen in Figs. 5 and 6. In cases where δ_{kn} has a considerable value, given the appearance of this term in both the numerator and denominator of Eq. (36), it is problematic to extract a single pattern for TED for 2D and 3D models.

In Fig. 7a, b, the impact of the Fourier and DPL models on TED versus geometrical ratio R_0/r_0 is examined for cases $n = 10$ and $n = 100$, respectively. In these curves it is supposed that $r_0 = 50 nm$. By observing these curves, it is reconfirmed that TED obtained in the framework of the DPL model has a smaller value compared to that computed based on the Fourier model. It is also obvious that for case $n = 10$ where the vibration mode number is relatively small, as the value of R_0/r_0 ascends and the parameter δ_{kn} reduces, both the effect of size and the effect of using a 2D or 3D model on TED value shrink.

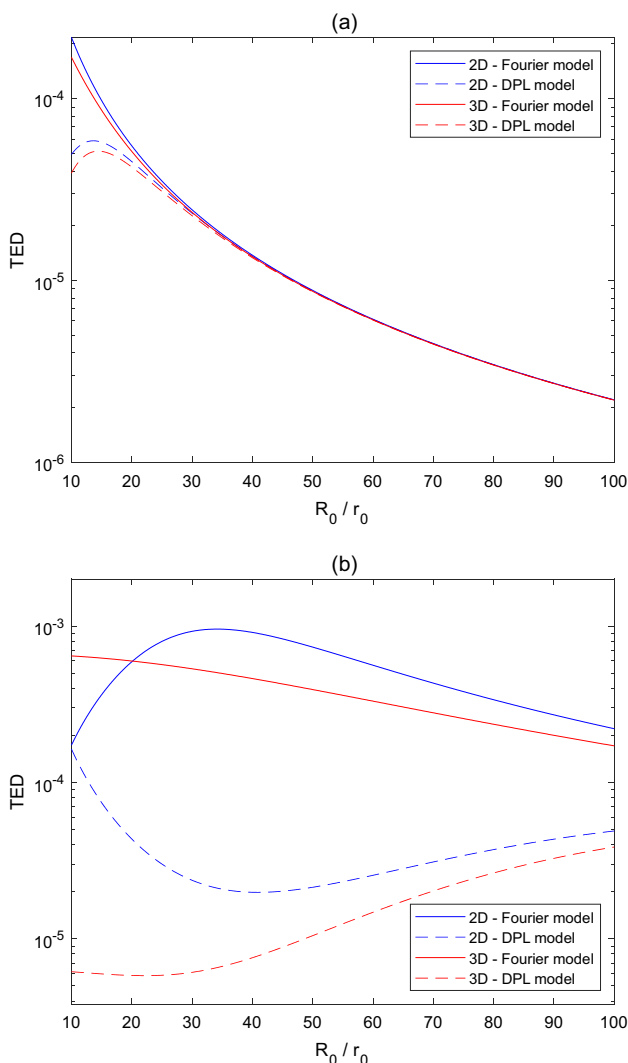**Fig. 7** The impact of the Fourier and DPL models on the variations of TED with respect to the geometrical ratio R_0/r_0 for $r_0 = 50$ nm **a** $n = 10$ **b** $n = 100$

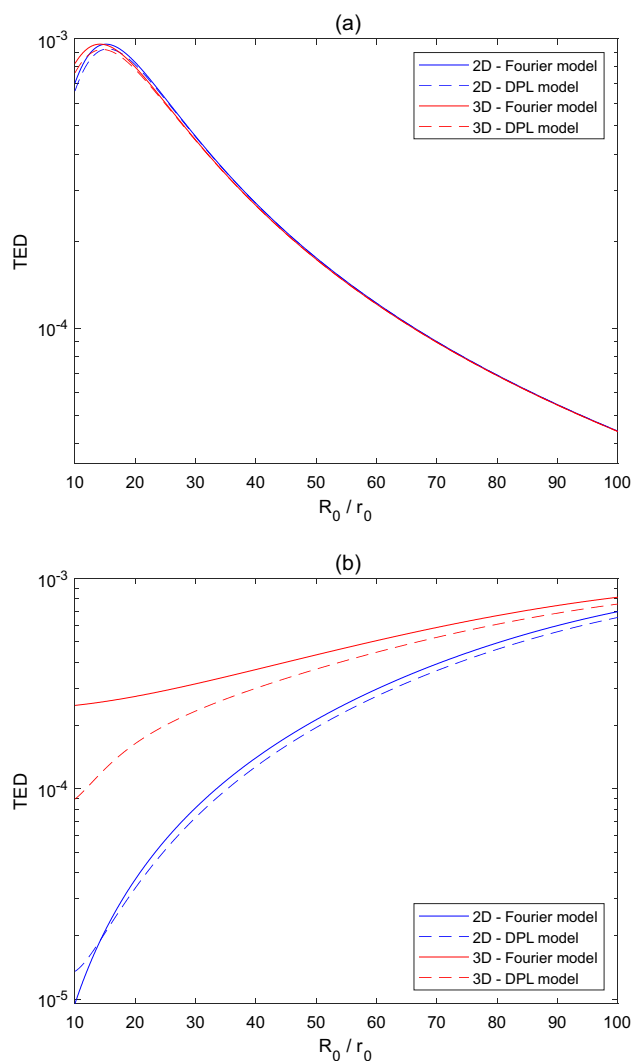**Fig. 8** The impact of the Fourier and DPL models on the variations of TED with respect to geometrical ratio R_0/r_0 for $r_0 = 1$ μm **a** $n = 10$ **b** $n = 100$

Figure 8a, b are drawn with the same conditions as Fig. 7a, b, with the only difference that in these figures it is assumed that $r_0 = 1$ μm. It can be seen again that for case $r_0 = 1$ μm, TED value calculated by 3D model is higher than that determined by 2D model. Besides, it is evident that by increasing the value of R_0/r_0, the effect of size weakens and the results of DPL model approach those of the Fourier model.

In Figs. 9 and 10, the dependence of TED value on the material of the ring is discussed. For this purpose, four materials gold (Au), copper (Cu), lead (Pb) and silver (Ag) at a reference temperature $T_0 = 300K$ are surveyed. In all these figures, the parameter r_0 is considered a fixed value of 400 nm. Figure 9a, b represent the variation of TED versus vibration mode number for 2D and 3D cases of heat conduction, respectively. In these figures, it is assumed that
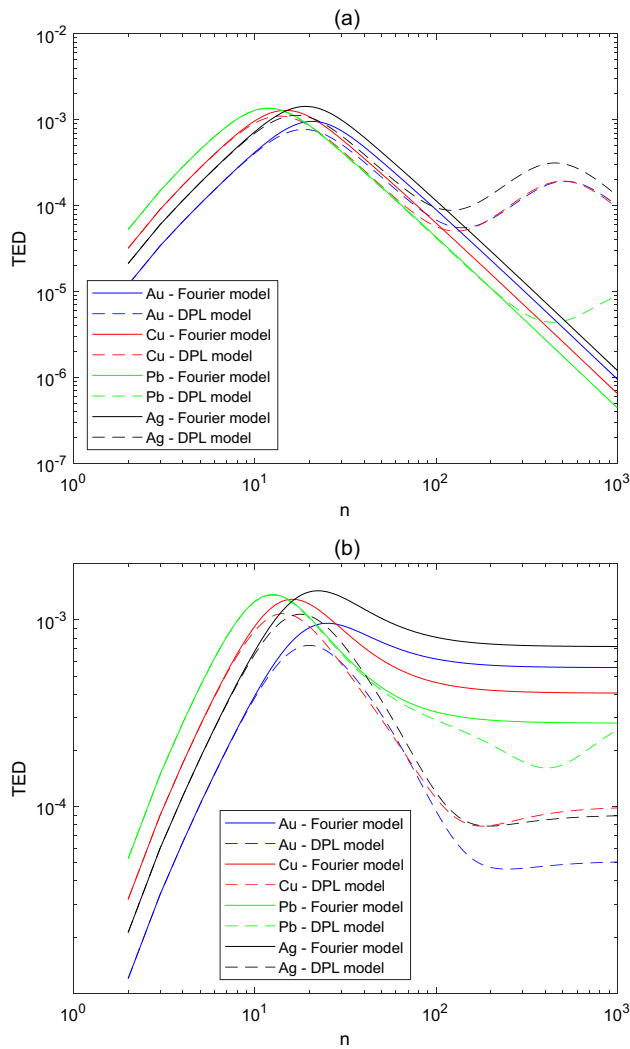
Fig. 9 The effect of material on the variations of TED versus vibration mode number for $r_0 = 400$ nm and $R_0 = 20r_0$ **a** 2D **b** 3D cases of heat conduction

Fig. 10 The effect of material on the variations of TED versus geometrical ratio R_0/r_0 for $r_0 = 400$ nm and $n = 20$ **a** 2D **b** 3D cases of heat conduction

$R_0 = 20r_0$. According to these figures, in low vibration modes (i.e. $n < 20$), TED in ascending order belongs to Au, Ag, Cu and Pb rings. In regard to the reason for this outcome one can say that the principal parameter that makes the coupling between structural and thermal domains is the thermal expansion coefficient α. Hence, greater amounts of α lead to more intensive thermoelastic coupling and higher levels of energy dissipation. Additionally, when phase lag parameters τ_q and τ_T take higher values, the impact of diffusion-type heat conduction dwindles. Consequently, for larger amounts of τ_q and τ_T, it is expected that the value of TED will be lower. In high mode numbers (i.e. almost $n > 50$), the highest value of TED occurs in rings made of Ag, Au, Cu and Pb, respectively. In Fig. 10a, b, the variation of TED as a function of the geometrical ratio R_0/r_0 is displayed for 2D and 3D models, respectively. These figures are plotted for mode
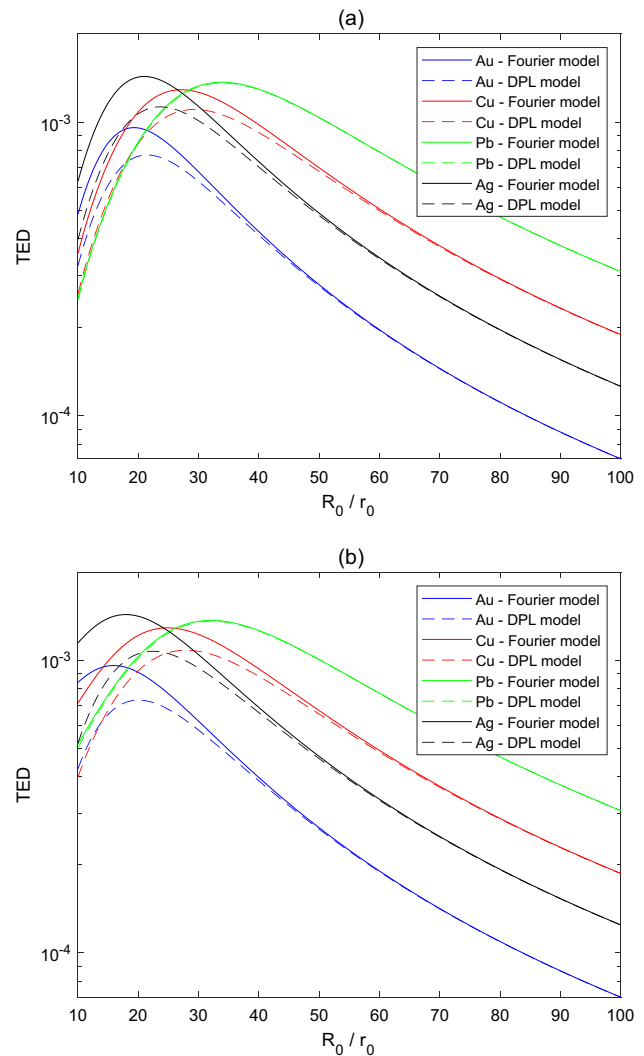
number $n = 20$. As it is apparent, for the range $R_0/r_0 < 30$, no specific rule can be mentioned for different materials, but for the range $R_0/r_0 > 30$, rings made of Pb, Cu, Ag and Au experience the highest amount of TED, respectively.

Conclusions

In the current article, by incorporating the size effect into the thermal domain by way of a dual-phase-lag (DPL) heat conduction model, 2D and 3D models has been developed for evaluating thermoelastic damping (TED) in micro/nanorings with circular cross section. To this aim, the equation of heat conduction obtained in the context of the DPL model has been solved first. Next, the temperature distribution in the ring has been extracted in the form of infinite series for 2D and 3D models of heat

transfer. Then, the definition of quality factor in entropy generation (EG) approach has been applied to establish an analytical relation containing the two-phase lag parameters of the DPL model for approximation of TED value in circular cross-sectional micro/nanorings. At the final stage, a thorough parametric study has been made to appraise the dependence of TED on some crucial factors like phase lag parameters of the DPL model, vibration mode number, geometrical parameters and material. The main concluding remarks can be stated as follows:

- Convergence analysis demonstrates that the inclusion of the first ten terms of a developed solution is adequate for the attainment of an accurate result.
- In general, the amount of TED estimated in the framework of the DPL model is lower than that predicted by the Fourier model. The greatest effect of the DPL model on TED can be seen in high vibration modes or smaller ring sizes (more precisely in nano dimensions).
- According to the definition of a parameter δ_{kn}, the difference between 2 and 3D models becomes noticeable in high vibration modes n and low geometrical ratios R_0/r_0.
- In the range of low values of vibration mode number n or high values of geometrical ratio R_0/r_0, the sensitivity of TED to dual-phase-lagging effect and 2D or 3D cases of heat conduction gets weak. Additionally, for very thin rings vibrating in the low mode numbers, TED is affected faintly by the DPL model and two or three-dimensionality of heat conduction.
- By the enlargement of cross-sectional radius r_0, the impact of size on the heat conduction field shrinks, so that the discrepancy between the predictions of the Fourier and DPL models descends.
- Among the examined materials, the maximum and minimum amount of TED in the low vibration modes occurs in the rings made of lead (Pb) and gold (Au), respectively.

Data availability The raw data required to reproduce these findings can be accessed by directly contacting the corresponding author.

Declarations

Conflict of interest There is no conflict of interest.

References

1. Ayazi F, Najafi K (2001) A HARPSS polysilicon vibrating ring gyroscope. J Microelectromech Syst 10(2):169–179
2. Tao Y, Wu X, Xiao D, Wu Y, Cui H, Xi X, Zhu B (2011) Design, analysis and experiment of a novel ring vibratory gyroscope. Sens Actuators A 168(2):286–299
3. Rourke AK, McWilliam S, Fox CHJ (2005) Frequency trimming of a vibrating ring-based multi-axis rate sensor. J Sound Vib 280(3–5):495–530
4. Hu ZX, Gallacher BJ, Burdess JS, Fell CP, Townsend K (2011) A parametrically amplified MEMS rate gyroscope. Sens Actuators A 167(2):249–260
5. Eley R, Fox CHJ, McWilliam S (2000) The dynamics of a vibrating-ring multi-axis rate gyroscope. Proc Inst Mech Eng C J Mech Eng Sci 214(12):1503–1513
6. Walter B, Faucher M, Algré E, Legrand B, Boisgard R, Aimé JP, Buchaillot L (2009) Design and operation of a silicon ring resonator for force sensing applications above 1 MHz. J Micromech Microeng 19(11):115009
7. Ding Y, Zhu X, Xiao S, Hu H, Frandsen LH, Mortensen NA, Yvind K (2015) Effective electro-optical modulation with high extinction ratio by a graphene–silicon microring resonator. Nano Lett 15(7):4393–4400
8. Zhou W, He J, Ran L, Chen L, Zhan L, Chen Q, Peng B (2021) A Piezoelectric Microultrasonic Motor With High Q and Good Mode Match. IEEE/ASME Trans Mechatron 26(4):1773–1781
9. Zangeneh-Nejad F, Safian R (2016) A graphene-based THz ring resonator for label-free sensing. IEEE Sens J 16(11):4338–4344
10. Li B, Lee C (2011) NEMS diaphragm sensors integrated with triple-nano-ring resonator. Sens Actuators A 172(1):61–68
11. Rajasekar R, Robinson S (2019) Nano-pressure and temperature sensor based on hexagonal photonic crystal ring resonator. Plasmonics 14(1):3–15
12. Roszhart TV (1990) The effect of thermoelastic internal friction on the Q of micromachined silicon resonators. In: IEEE 4th Technical Digest on Solid-State Sensor and Actuator Workshop, pp 13–16. IEEE
13. Duwel A, Gorman J, Weinstein M, Borenstein J, Ward P (2003) Experimental study of thermoelastic damping in MEMS gyros. Sens Actuators, A 103(1–2):70–75
14. Lord HW, Shulman Y (1967) A generalized dynamical theory of thermoelasticity. J Mech Phys Solids 15(5):299–309
15. Guyer RA, Krumhansl JA (1966) Solution of the linearized phonon Boltzmann equation. Phys Rev 148(2):766
16. Tzou DY (2014) Macro-to microscale heat transfer: the lagging behavior. Wiley
17. Zener C (1937) Internal friction in solids. I. Theory of internal friction in reeds. Phys Rev 52(3):230
18. Lifshitz R, Roukes ML (2000) Thermoelastic damping in micro- and nanomechanical systems. Phys Rev B 61(8):5600
19. Borjalilou V, Asghari M, Taati E (2020) Thermoelastic damping in nonlocal nanobeams considering dual-phase-lagging effect. J Vib Control 26(11–12):1042–1053
20. Jalil AT, Saleh ZM, Imran AF, Yasin Y, Ruhaima AAK, Gatea A, Esmaeili S (2022) A size-dependent generalized thermoelasticity theory for thermoelastic damping in vibrations of nanobeam resonators. Int J Struct Stab Dyn. https://doi.org/10.1142/S021945542350133X
21. Abbas IA, Hobiny AD (2016) Analytical solution of thermoelastic damping in a nanoscale beam using the fractional order theory of thermoelasticity. Int J Struct Stab Dyn 16(09):1550064
22. Mamen B, Bouhadra A, Bourada F, Bourada M, Tounsi A, Mahmoud SR, Hussain M (2022) Combined effect of thickness stretching and temperature-dependent material properties on dynamic behavior of imperfect FG beams using three variable quasi-3D model. J Vib Eng Technol 10:1–23
23. Esfahani S, Khadem SE, Mamaghani AE (2019) Nonlinear vibration analysis of an electrostatic functionally graded nano-resonator with surface effects based on nonlocal strain gradient theory. Int J Mech Sci 151:508–522

24. Hossain M, Lellep J (2022) Natural vibration of axially graded multi-cracked nanobeams in thermal environment using power series. J Vib Eng Technol 10:1–18

25. Yue X, Yue X, Borjalilou V (2021) Generalized thermoelasticity model of nonlocal strain gradient Timoshenko nanobeams. Arch Civ Mech Eng 21(3):1–20

26. Borjalilou V, Asghari M (2021) Size-dependent analysis of thermoelastic damping in electrically actuated microbeams. Mech Adv Mater Struct 28(9):952–962

27. Singh B, Kumar H, Mukhopadhyay S (2021) Thermoelastic damping analysis in micro-beam resonators in the frame of modified couple stress and Moore–Gibson–Thompson (MGT) thermoelasticity theories. Waves Random Complex Media 31:1–18

28. Zhao G, Shi S, Gu B, He T (2022) Thermoelastic damping analysis to nano-resonators utilizing the modified couple stress theory and the memory-dependent heat conduction model. J Vib Eng Technol 10(2):715–726

29. Borjalilou V, Asghari M, Bagheri E (2019) Small-scale thermoelastic damping in micro-beams utilizing the modified couple stress theory and the dual-phase-lag heat conduction model. J Therm Stresses 42(7):801–814

30. Numanoğlu HM, Ersoy H, Akgöz B, Civalek Ö (2022) A new eigenvalue problem solver for thermo-mechanical vibration of Timoshenko nanobeams by an innovative nonlocal finite element method. Math Methods Appl Sci 45(5):2592–2614

31. Ghayesh MH, Farokhi H (2015) Thermo-mechanical dynamics of three-dimensional axially moving beams. Nonlinear Dyn 80(3):1643–1660

32. Liu D, Geng T, Wang H, Esmaeili S (2021) Analytical solution for thermoelastic oscillations of nonlocal strain gradient nanobeams with dual-phase-lag heat conduction. Mech Based Des Struct Mach 49:1–31

33. Ebrahimi-Mamaghani A, Sotudeh-Gharebagh R, Zarghami R, Mostoufi N (2022) Thermo-mechanical stability of axially graded Rayleigh pipes. Mech Based Des Struct Mach 50(2):412–441

34. Abouelregal AE, Ersoy H, Civalek Ö (2021) A new heat conduction model for viscoelastic micro beams considering the magnetic field and thermal effects. Waves in Random Complex Media 31:1–30

35. Lu ZQ, Liu WH, Ding H, Chen LQ (2022) Energy transfer of an axially loaded beam with a parallel-coupled nonlinear vibration isolator. J Vib Acoust 144(5):051009. https://doi.org/10.1115/1.4054324

36. Gu B, He T (2021) Investigation of thermoelastic wave propagation in Euler-Bernoulli beam via nonlocal strain gradient elasticity and GN theory. J Vib Eng Technol 9(5):715–724

37. Bai X, Shi H, Zhang K, Zhang X, Wu Y (2022) Effect of the fit clearance between ceramic outer ring and steel pedestal on the sound radiation of full ceramic ball bearing system. J Sound Vib 529:116967. https://doi.org/10.1016/j.jsv.2022.116967

38. Ghayesh MH (2019) Viscoelastic mechanics of Timoshenko functionally graded imperfect microbeams. Compos Struct 225:110974

39. Sarparast H, Alibeigloo A, Borjalilou V, Koochakianfard O (2022) Forced and free vibrational analysis of viscoelastic nanotubes conveying fluid subjected to moving load in hygro-thermo-magnetic environments with surface effects. Arch Civ Mech Eng 22(4):1–28

40. Ebrahimi F, Seyfi A, Nouraei M, Haghi P (2022) Influence of magnetic field on the wave propagation response of functionally graded (FG) beam lying on elastic foundation in thermal environment. Waves Random Complex Media 32(5):2158–2176

41. Guo Z, Yang J, Tan Z, Tian X, Wang Q (2021) Numerical study on gravity-driven granular flow around tube out-wall: Effect of tube inclination on the heat transfer. Int J Heat Mass Transf 174:121296. https://doi.org/10.1016/j.ijheatmasstransfer.2021.121296

42. Weng W, Lu Y, Borjalilou V (2021) Size-dependent thermoelastic vibrations of Timoshenko nanobeams by taking into account dual-phase-lagging effect. Eur Phys J Plus 136(7):1–26

43. Selvamani R, Rexy JB, Ebrahimi F (2022) Finite element modeling and analysis of piezoelectric nanoporous metal foam nanobeam under hygro and nonlinear thermal field. Acta Mech 233(8):3113–3132

44. Zheng C, An Y, Wang Z, Wu H, Qin X, Eynard B, Zhang Y (2022) Hybrid offline programming method for robotic welding systems. Robot Comput-Integr Manuf 73:102238. https://doi.org/10.1016/j.rcim.2021.102238

45. Borjalilou V, Taati E, Ahmadian MT (2019) Bending, buckling and free vibration of nonlocal FG-carbon nanotube-reinforced composite nanobeams: exact solutions. SN Appl Sci 1(11):1–15

46. Sarparast H, Ebrahimi-Mamaghani A (2019) Vibrations of laminated deep curved beams under moving loads. Compos Struct 226:111262

47. Taati E, Borjalilou V, Fallah F, Ahmadian MT (2022) On size-dependent nonlinear free vibration of carbon nanotube-reinforced beams based on the nonlocal elasticity theory: perturbation technique. Mech Based Des Struct Mach 50(6):2124–2146

48. Ebrahimi-Mamaghani A, Mostoufi N, Sotudeh-Gharebagh R, Zarghami R (2022) Vibrational analysis of pipes based on the drift-flux two-phase flow model. Ocean Eng 249:110917

49. Khaniki HB, Ghayesh MH, Chin R, Chen LQ (2022) Experimental characteristics and coupled nonlinear forced vibrations of axially travelling hyperelastic beams. Thin-Walled Struct 170:108526

50. Kumar H, Mukhopadhyay S (2020) Thermoelastic damping analysis for size-dependent microplate resonators utilizing the modified couple stress theory and the three-phase-lag heat conduction model. Int J Heat Mass Transf 148:118997

51. Ge X, Li P, Fang Y, Yang L (2021) Thermoelastic damping in rectangular microplate/nanoplate resonators based on modified nonlocal strain gradient theory and nonlocal heat conductive law. J Therm Stresses 44(6):690–714

52. Sharma LK, Grover N, Bhardwaj G (2022) Buckling and free vibration analysis of temperature-dependent functionally graded CNT-reinforced plates. J Vib Eng Technol 10:1–18

53. Yang Z, Cheng D, Cong G, Jin D, Borjalilou V (2021) Dual-phase-lag thermoelastic damping in nonlocal rectangular nanoplates. Waves in Random Complex Media 31:1–20

54. Li F, Esmaeili S (2021) On thermoelastic damping in axisymmetric vibrations of circular nanoplates: incorporation of size effect into structural and thermal areas. The European Physical Journal Plus 136(2):1–17

55. Zenkour AM, Abouelregal AE (2018) A three-dimensional generalized shock plate problem with four thermoviscoelastic relaxations. Can J Phys 96(8):938–954

56. Rajasekaran S, Khaniki HB, Ghayesh MH (2022) Thermo-mechanics of multi-directional functionally graded elastic sandwich plates. Thin-Walled Struct 176:109266

57. Li FL, Fan SJ, Hao YX, Yang L, Lv M (2022) Dynamic behaviors of thermal–electric imperfect functionally graded piezoelectric sandwich microplates based on modified couple stress theory. J Vib Eng Technol 10:1–15

58. Abbas IA, Alzahrani FS (2018) A Green-Naghdi model in a 2D problem of a mode I crack in an isotropic thermoelastic plate. Phys Mesomech 21(2):99–103

59. Soni S, Jain NK, Joshi PV, Gupta A (2020) Effect of fluid-structure interaction on vibration and deflection analysis of generally orthotropic submerged micro-plate with crack under thermal environment: an analytical approach. J Vib Eng Technol 8(5):643–672

60. Safaei B, Moradi-Dastjerdi R, Qin Z, Chu F (2019) Frequency-dependent forced vibration analysis of nanocomposite sandwich plate under thermo-mechanical loads. Compos B Eng 161:44–54

61. Esen I, Özmen R (2022) Thermal vibration and buckling of magneto-electro-elastic functionally graded porous nanoplates using nonlocal strain gradient elasticity. Compos Struct 296:115878

62. Dangi C, Lal R (2022) Nonlinear thermal effect on free vibration of FG rectangular mindlin nanoplate of bilinearly varying thickness via Eringen's nonlocal theory. J Vib Eng Technol 10:1–19

63. Sh EL, Kattimani S, Vinyas M (2022) Nonlinear free vibration and transient responses of porous functionally graded magneto-electro-elastic plates. Arch Civ Mech Eng 22(1):1–26

64. Ghayesh MH, Farokhi H, Gholipour A, Tavallaeinejad M (2018) Nonlinear oscillations of functionally graded microplates. Int J Eng Sci 122:56–72

65. Kumar P, Harsha SP (2022) Static, buckling and vibration response analysis of three-layered functionally graded piezoelectric plate under thermo-electric mechanical environment. J Vib Eng Technol 10:1–38

66. Singh B, Kumar H, Mukhopadhyay S (2022) Analysis of size effects on thermoelastic damping in the Kirchhoff's plate resonator under Moore–Gibson–Thompson thermoelasticity. Thin-Walled Struct 180:109793

67. Chugh N, Partap G (2021) Study of thermoelastic damping in microstretch thermoelastic thin circular plate. J Vib EngTechnol 9(1):105–114

68. Xiao C, Zhang G, Hu P, Yu Y, Mo Y, Borjalilou V (2021) Size-dependent generalized thermoelasticity model for thermoelastic damping in circular nanoplates. Waves in Random Complex Media 31:1–21

69. Yani A, Abdullaev S, Alhassan MS, Sivaraman R, Jalil, AT (2023) A non-Fourier and couple stress-based model for thermoelastic dissipation in circular microplates according to complex frequency approach. In J Mech Mater Des 19:1–24

70. Arefi M, Zenkour AM (2018) Size-dependent thermoelastic analysis of a functionally graded nanoshell. Mod Phys Lett B 32(03):1850033

71. Alshenawy R, Sahmani S, Safaei B, Elmoghazy Y, Al-Alwan A, Al Nuwairan M (2023) Three-dimensional nonlinear stability analysis of axial-thermal-electrical loaded FG piezoelectric microshells via MKM strain gradient formulations. Appl Math Comput 439:127623

72. Kim JH, Kim JH (2019) Phase-lagging of the thermoelastic dissipation for a tubular shell model. Int J Mech Sci 163:105094

73. Rao R, Ye Z, Yang Z, Sahmani S, Safaei B (2022) Nonlinear buckling mode transition analysis of axial–thermal–electrical-loaded FG piezoelectric nanopanels incorporating nonlocal and couple stress tensors. Arch Civ Mech Eng 22(3):1–21

74. Song J, Wu D, Arefi M (2022) Modified couple stress and thickness-stretching included formulation of a sandwich micro shell subjected to electro-magnetic load resting on elastic foundation. Defence Technol. https://doi.org/10.1016/j.dt.2022.04.015

75. Ghayesh MH, Farokhi H (2017) Nonlinear mechanics of doubly curved shallow microshells. Int J Eng Sci 119:288–304

76. Kumar A, Kumar D, Sharma K (2021) An analytical investigation on linear and nonlinear vibrational behavior of stiffened functionally graded shell panels under thermal environment. J Vib Eng Technol 9(8):2047–2071

77. Li M, Cai Y, Fan R, Wang H, Borjalilou V (2022) Generalized thermoelasticity model for thermoelastic damping in asymmetric vibrations of nonlocal tubular shells. Thin-Walled Struct 174:109142

78. Banerjee R, Rout M, Karmakar A, Bose D (2022) Free vibration response of rotating hybrid composite conical shell under hygrothermal conditions. J VibEng Technol 10:1–18

79. Li M, Cai Y, Bao L, Fan R, Zhang H, Wang H, Borjalilou V (2022) Analytical and parametric analysis of thermoelastic damping in circular cylindrical nanoshells by capturing small-scale effect on both structure and heat conduction. Arch Civ Mech Eng 22(1):1–16

80. Liu H, Sahmani S, Safaei B (2022) Nonlinear buckling mode transition analysis in nonlocal couple stress-based stability of FG piezoelectric nanoshells under thermo-electromechanical load. Mech Adv Mater Struct 29:1–21

81. Khaniki HB, Ghayesh MH (2023) Highly nonlinear hyperelastic shells: Statics and dynamics. Int J Eng Sci 183:103794

82. Wong SJ, Fox CHJ, McWilliam S (2006) Thermoelastic damping of the in-plane vibration of thin silicon rings. J Sound Vib 293(1–2):266–285

83. Fang Y, Li P (2015) Thermoelastic damping in thin microrings with two-dimensional heat conduction. Phys E 69:198–206

84. Li P, Fang Y, Zhang J (2016) Thermoelastic damping in microrings with circular cross-section. J Sound Vib 361:341–354

85. Kim JH, Kim JH (2018) Mass imperfections in a toroidal microring model with thermoelastic damping. Appl Math Model 63:405–414

86. Tai Y, Chen N (2019) Thermoelastic damping in the out-of-plane vibration of a microring resonator with rectangular cross-section. Int J Mech Sci 151:684–691

87. Zhou H, Li P, Fang Y (2019) Single-phase-lag thermoelastic damping models for rectangular cross-sectional micro-and nano-ring resonators. Int J Mech Sci 163:105132

88. Zhou H, Li P (2021) Dual-phase-lagging thermoelastic damping and frequency shift of micro/nano-ring resonators with rectangular cross-section. Thin-Walled Structures 159:107309

89. Kim JH, Kim JH (2021) Thermoelastic attenuation of circular-cross-sectional micro/nanoring including single-phase-lag time. Int J Mech Mater Des 17(4):915–929

90. Ge Y, Sarkar, A (2022) Thermoelastic damping in vibrations of small-scaled rings with rectangular cross-section by considering size effect on both structural and thermal domains. Int J Struct Stab Dyn 23:2350026

91. Chen H, Liu M, Chen Y, Li S, Miao Y (2022) Nonlinear lamb wave for structural incipient defect detection with sequential probabilistic ratio test. Secur Commun Netw. https://doi.org/10.1155/2022/9851533

92. Chen H, Li S (2022) Collinear nonlinear mixed-frequency ultrasound with FEM and experimental method for structural health prognosis. Processes 10(4):656. https://doi.org/10.3390/pr10040656

93. Gong X, Wang L, Mou Y, Wang H, Wei X, Zheng W, Yin L (2022) Improved Four-channel PBTDPA control strategy using force feedback bilateral teleoperation system. Int J Control Autom Syst 20(3):1002–1017. https://doi.org/10.1007/s12555-021-0096-y

94. Sharma DK, Mittal H (2020) Analysis of free vibrations of axisymmetric functionally graded generalized viscothermoelastic cylinder using series solution. J Vib Eng Technol 8(6):783–798

95. Cheng Z, Guo Z, Fu P, Yang J, Wang Q (2021) New insights into the effects of methane and oxygen on heat/mass transfer in reactive porous media. Int Commun Heat Mass Transf 129:105652. https://doi.org/10.1016/j.icheatmasstransfer.2021.105652

96. Wang J, Tian J, Zhang X, Yang B, Liu S, Yin L, Zheng W (2022) Control of time delay force feedback teleoperation system with finite time convergence. Front Neurorobot. https://doi.org/10.3389/fnbot.2022.877069

97. Sharma DK, Bachher M, Sharma MK, Sarkar N (2021) On the analysis of free vibrations of nonlocal elastic sphere of FGM type in generalized thermoelasticity. J Vib Eng Technol 9(1):149–160

98. Zhang J, Zhang C, Xue Q (2022) Insight into energy dissipation behavior of a SDOF structure controlled by the pounding tuned

mass damper system. Earthq Eng Struct Dynam 51(4):958–973. https://doi.org/10.1002/eqe.3599

99. Nowick AS (2012) Anelastic relaxation in crystalline solids (Vol. 1). Elsevier